Electronic Supporting Information

Nanoparticles as a Hedgehog signaling inhibitor for the suppression of cancer growth and metastasis

Zhaojian Xu,[‡a] Manjing Li,[‡a] Rong Sun,[a] Binbin Chu,[a] Bin Song,[a] Houyu Wang,[a] Yuanyuan Su*[b] and Yao He*[a]

[a]Laboratory of Nanoscale Biochemical Analysis, Institute of Functional Nano and Soft Materials (FUNSOM) and Collaborative Innovation Center of Suzhou Nano Science and Technology, Soochow University, Suzhou 215123, China

[b]Guangdong Provincial Key Laboratory of Malignant Tumor Epigenetics and Gene Regulation, Medical Research Center, Sun Yat-Sen Memorial Hospital, Sun Yat-Sen University, Guangzhou 510120, China

*E-mail: suyy36@mail.sysu.edu.cn; yaohe@suda.eud.cn

Table of Contents

1. Reagents and apparatus S3
2. Methods S4
3. Characterizations of SiNPs. S6
4. The stability of SiNPs in different pH values. S7
5. LDH level and ATP content of NIH3T3 cells treated with SiNPs. S7
6. Biodistribution of SiNPs *in vivo* S8
7. H&E staining images of main organs of mice treated with SiNPs S9
8. Effects of SiNPs on NF-κB, AKT, and MAPK/ERK signaling pathways S10
9. Cell uptake study of SiNPs S12
10. Inhibition of SiNPs on HH signaling pathway in LNCaP cells S13
11. The high-resulution images of filopodia. S13
12. Wound healing of PC3 cells treated with SiNPs S14
13. Semi-quantitative results of transwell migration and invasion S15
14. The degree of lung metastasis in tumor model of PC3 prostate cancer. S16
15. *Gli1* mRNA expression at tumor site S17
16. References S17

1. Reagents and apparatus

Reagents. These (3-Aminopropyl) trimethoxysilane, 1,8-naphthalimide, antibody, 3-(4,5-dimethylthiazol-2-yl)-2,5-diphenyltetrazolium bromide (MTT), and Alexa Fluor 633-labeled second antibody are purchased from Sigma-Aldrich (Shanghai, China). Cell Titer-Glo Luminescent (CTG) Cell Viability Assay kit is obtained from Promega (Beijing, China). PrimeScript™ RT Master Mix and SYBR Green Master Mix kit are purchased from Roche (Shanghai, China). Dulbecco's modified eagle media (DMEM), fetal bovine serum, penicillin (100 μg/mL), streptomycin (100 μg/mL), and PBS solution are obtained from Invitrogen corporation (Life Technologies, Shanghai, China). The 1,1'-dioctadecyl-3,3,3',3'-tetramethylindodicarbocyanine perchlorate (DiD) membrane tracker solution is obtained from AmyJet Scientific Incorporation (Wuhan, China). All chemicals are analytical grade and used without additional purification. All solutions are prepared using ultrapure water (Millipore) throughout the work. All animal experimental procedures are performed according to the Guideline for Animal Experimentation with the approval of the animal care committee of Soochow University.

Apparatus. The morphology and size of SiNPs are examined by transmission electronic microscopy (TEM, Philips CM 200) with 200 kV. A 750 UV-vis-near-infrared spectrophotometer (Perkin-Elmer lambda) is used for the measurement of UV-vis absorption spectra. A spectro-fluorimeter (HORIBA JOBIN YVON FLUORMAX-4) is employed for recording photoluminescence (PL). Delsa™ nano submicron particle size is employed for the analysis of dynamic light scattering (DLS). Fluorescence imaging experiments are performed by a confocal laser scanning microscope (CLSM, Leica, TCS-SP5 II). Flow analysis images are obtained by a flow cytometry (FCM, BD, FACS Calibur). *In vivo* fluorescence images are obtained by an *in vivo* optical imaging system (IVIS Lumina III, PerkinElme).

2. Methods

Cellular internalization of SiNPs. Cellular internalization of SiNPs was analyzed by CLSM and FCM. For CLSM imaging, glass slide was placed per well in 24-well plate, and then 5×10^4 cells were planted per well overnight. After incubated with 700 μg/mL SiNPs for different periods of time, the cell membrane was stained with DiD for 30 min. Before photographed with CLSM, the cells were washed 3 times with PBS. For FCM detection, 6-well plate was planted with 2×10^5 cells per well overnight. After incubated with 700 μg/mL SiNPs for different periods of time, the cells were washed 3 times with PBS and detected by FCM.

Wound healing assay. PC3 cells were cultured in 35 mm petri dishes overnight at a density of approximate 3×10^5 cells per well. When the cells were confluent, the cell monolayer was scratched with 200 μL pipette tip. Subsequently, it is washed 3 times with PBS to remove cell debris. After scratching, complete medium containing different concentrations (0, 180, 350 and 700 μg/mL) of SiNPs were added to the petri dishes for 24 h. At last, the cells were observed with microscope.

Immunofluorescence staining. In 24-well plate, 5×10^4 cells per well were cultured overnight. After treated with SiNPs for 24 h, the cells were fixed with 4% paraformaldehyde. Then, the cells were treated with 0.1% Triton X-100 solution at 37 °C for 40 min after washed 3 times with PBS. Thereafter, the cells were incubated with the antibody (diluted 1:500). Afterwards, the cells were incubated with the Alexa Fluor 633-labeled second antibody (diluted 1:1000). To label actin filaments, the cells were treated with rhodamine-labeled phalloidin. At last, the nuclei was stained with 10 μg/mL Hochest 33258. Images were taken by confocal laser scanning microscope (CLSM).

Primer. Mouse GAPDH: 5′-ACT GGC ATG GCC TTC CG-3′ (forward) and 5′-CAG GCG GCA CGT CAG ATC-3′ (reverse); human GAPDH: 5′-ACT TTG GTA TCG TGG AAG GACT-3′ (forward) and 5′-GTA GAG GCA GGG ATG ATG TTCT-3′ (reverse); mouse Ptch1: 5′-GCC TTC GCT GTG GGA TTA AAG-3′ (forward) and 5′-CTT CTC CTA TCT TCT GAC GGGT-3′ (reverse); human Ptch1: 5′-GAA GAA GGT GCT AAT GTC CTG AC-3′ (forward) and 5′-GTC CCA GAC TGT AAT TTC GCC-

3′ (reverse); mouse Gli1: 5′-CCA AGC CAA CTT TAT GTC AGGG-3′ (forward) and 5′-AGC CCG CTT CTT TGT TAA TTT GA-3′ (reverse); human Gli1:5′-AGC GTG AGC CTG AAT CTG TG-3′ (forward) and 5′-CAG CAT GTA CTG GGC TTT GAA-3′ (reverse); mouse TNFα: 5′-CCT GTA GCC CAC GTC GTA G-3′ (forward) and 5′-GGG AGT AGA CAA GGT ACA ACC C-3′ (reverse); mouse iNOS: 5′-GTT CTC AGC CCA ACA ATA CAA GA-3′ (forward) and 5′-GTG GAC GGG TCG ATG TCA C-3′ (reverse); mouse CD86: 5′-CTG GAC TCT ACG ACT TCA CAA TG-3′ (forward) and 5′-AGT TGG CGA TCA CTG ACA GTT-3′ (reverse); mouse Arg-1: 5′-GAC CGT TGT GTG TGT TCT GG-3′ (forward) and 5′-GAT GAG CAG CAT CAC AAG GA-3′ (reverse); mouse IL-10: 5′-ACT GGC ATG AGG ATC AGC AG-3′ (forward) and 5′-CTC CTT GAT TTC TGG GCC AT-3′ (reverse); mouse CD206: 5′-CTG CAG ATG GGT GGG TTA TT-3′ (forward) and 5′-GGC ATT GAT GCT GCT GTT ATG-3′ (reverse).

3. Characterizations of SiNPs.

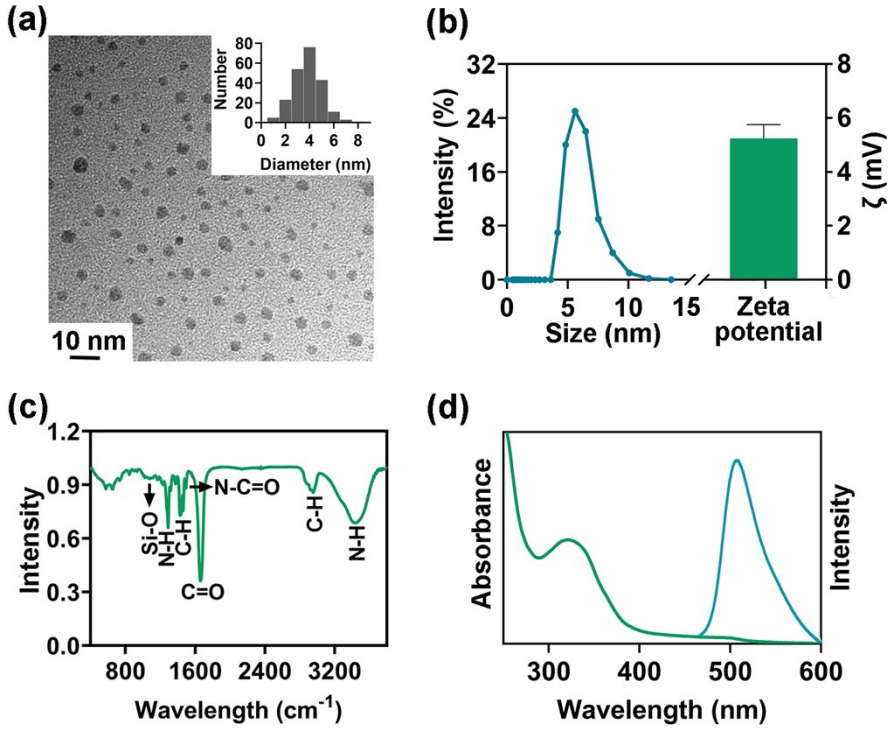

Fig. S1 Characterizations of SiNPs. (a) TEM image and corresponding size distribution (inset) of SiNPs. (b) DLS diameter distribution and zeta potential of SiNPs. (c) The FTIR spectrum shows surface chemical bonding of SiNPs. (d) UV-vis absorbance and PL spectra of SiNPs.

According to TEM images in Fig. S1a, SiNPs exhibit spherical shape. By measuring more than 200 particles in TEM images, the diameter of SiNPs is measured to be 3.8 ± 0.5 nm. The hydrodynamic diameter of SiNPs is ~ 6.7 nm as determined by DLS (Fig. S1b). The zeta potential result shows that the surface of the SiNPs is ~ 5.2 ± 0.5 mV. Strong absorbance peaks at 1080, 1290, 1421-1440, 1525, 1664, 2958 and 3470 cm^{-1} are credited to the vibrational stretch of Si-O bonding, N-H deformation vibration, the C-H aromatic skeletal vibration, N-C=O vibration, C=O stretching vibration, C-H vibration, and the N-H stretching vibration, respectively. (Fig. S1c). UV-vis absorbance and PL spectra show absorption and emission peaks of SiNPs are 325 nm and 510 nm, respectively (Fig. S1d).

4. The stability of SiNPs in different pH values.

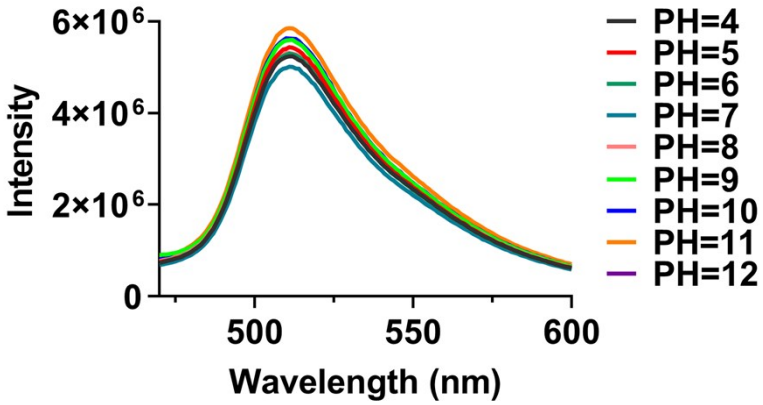

Fig. S2 The stability of SiNPs in different pH values. PL spectra of SiNPs at different pH conditions (pH= 4, 5, 6, 7, 8, 9, 10, 11 and 12).

The fluorescence intensity of SiNPs shows feeble change in pH values ranging 4-12, indicating that SiNPs have good pH stability and are beneficial for biological applications.

5. LDH level and ATP content of NIH3T3 cells treated with SiNPs.

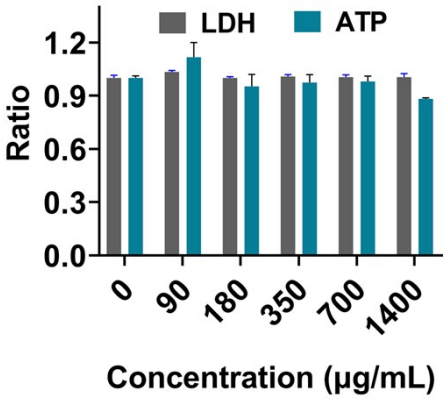

Fig. S3 LDH level and ATP content of NIH3T3 cells treated with SiNPs. ATP level and LDH content of NIH3T3 cells exposed to different concentrations of SiNPs for 48 h.

LDH and ATP assays are used to quantitatively study the effects of SiNPs on cell membrane integrity and cell metabolism, respectively. As shown in Fig. S3, LDH content and ATP level of NIH3T3 cells have no obvious change after treatment with SiNPs, implying that SiNPs have good biocompatibility *in vitro*.

6. Biodistribution of SiNPs *in vivo*

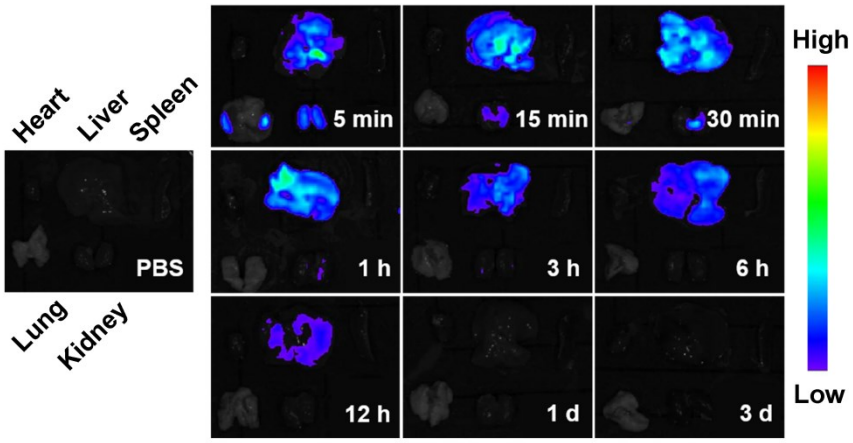

Fig. S4 Biodistribution of SiNPs *in vivo*. Images monitored by IVIS of the main organs (heart, liver, spleen, lung, and kidney) in mice after intravenous injection of 12.5 mg/kg SiNPs at different time points (5, 15, and 30 min, 1, 3, 6, and 12 h, 1 and 3 d).

After subtracting the background fluorescence signal from the control group (PBS-injected), we found that a large amount of accumulation in the liver and kidney after 5 min of intravenous injection and a small amount in the lung. With the prolongation of time (15 min - 12 h), the fluorescence signal of SiNPs reduced greatly. However, the fluorescence signal was still distributed in the liver and kidney. After 1 d, the signal of SiNPs in main organs was undetectable.

7. H&E staining images of main organs of mice treated with SiNPs

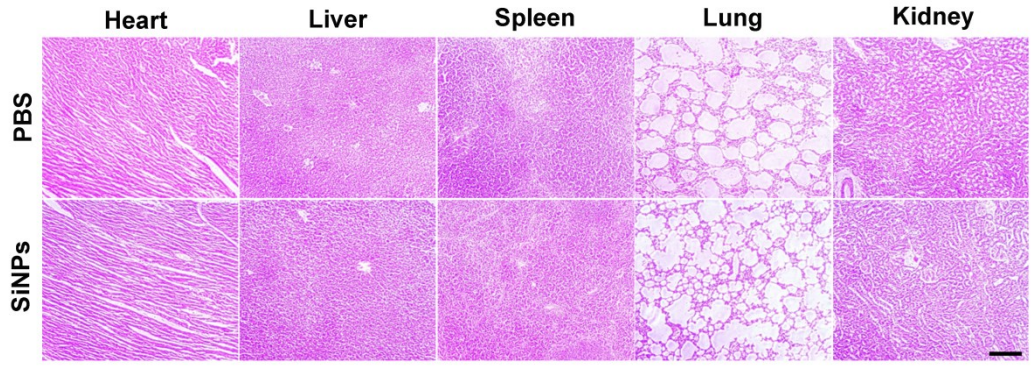

Fig. S5 H&E staining images of main organs (heart, liver, spleen, lung, and kidney) of mice after intravenous injection of 12.5 mg/kg SiNPs for 7 d. Scale bar = 100 μm.

The morphology of the tissue cells in the SiNPs group was similar to that of the PBS group, in which the liver cells were normal in morphology and showed no signs of inflammatory infiltration. There were no morphological changes in the kidney tissue samples, and the glomerular structure was clearly visible without obvious swelling. No watery degeneration was observed; no inflammation, fibrosis, or granuloma were found in the lungs; no cell necrosis was found in all tissue section.

8. Effects of SiNPs on NF-κB, AKT, and MAPK/ERK signaling pathways

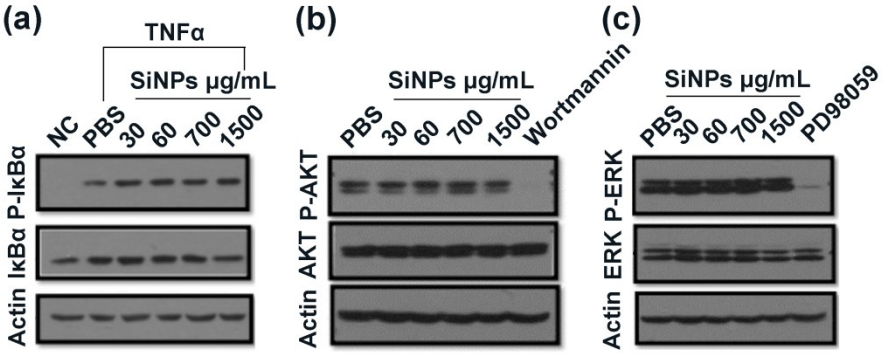

Fig. S6 The effects of SiNPs on NF-κB, AKT, and MAPK/ERK signaling pathways. (a) Panc-1 cells are treated with SiNPs for 24 h and then treated with TNFα. Cell lysate is collected for western blotting analysis. (b) Panc-1 cells are treated with SiNPs for 24 h and then cell lysate is collected for western blotting analysis. The negative control is cells without any treatment, and the positive control is cells treated with wortmannin. (c) Panc-1 cells are treated with SiNPs for 24 h and then cell lysate is collected for western blotting analysis. The negative control is cells without any treatment, and the positive control is cells treated with with PD98059.

NF-κB, AKT, and MAPK/ERK signaling pathways are closely related to cell proliferation.[1-3] In order to analyze the influence of SiNPs on NF-κB, AKT, and MAPK/ERK signaling pathways, in addition to SiNPs (700 and 1500 μg/mL) synthesized by photochemical methods, we also selected SiNPs (30 and 60 μg/mL) prepared by microwave methods[4] for comprehensively evaluating the influence of SiNPs on NF-κB, AKT, and ERK signaling pathways. For NF-κB signaling pathway, Panc-1 cells were first incubated with two kinds of SiNPs for 24 h and then treated with TNFα (40 ng/mL) for 10 min to activate the NF-κB signaling pathway. After that, we detected the protein level of phosphorylated IκBα and IκBα in the cells by western blotting (Fig. S6a). The phosphorylated IκB protein level in Panc-1 cells treated with the two kinds of SiNPs showed no significant changes compared with the PBS group. For AKT signaling pathway, compared with Panc-1 cells treated with the positive control inhibitor wortmannin (1 μg/mL) for 8 h, the phosphorylated AKT protein content is not significantly observed after treatment with two kinds of SiNPs for 24 h,

showing that two kinds of SiNPs have no significant inhibitory effect on AKT signaling pathway in Panc-1 cells (Fig. S6b). For MAPK/ERK signaling pathway, the result showed that the phosphorylated ERK protein content of the Panc-1 cells had no obvious change after treatment with two kinds of SiNPs for 24 h (Fig. S6c). Phosphorylated ERK protein level was significantly reduced in cells treated inhibitor PD98059 (100 μM) for 10 h. Therefore, the two kinds of SiNPs have no significant inhibitory effect on the intracellular MAPK/ERK signaling pathway. In short, SiNPs had no obvious effect on NF-κB, AKT, and MAPK/ERK signaling pathways.

9. Cell uptake study of SiNPs

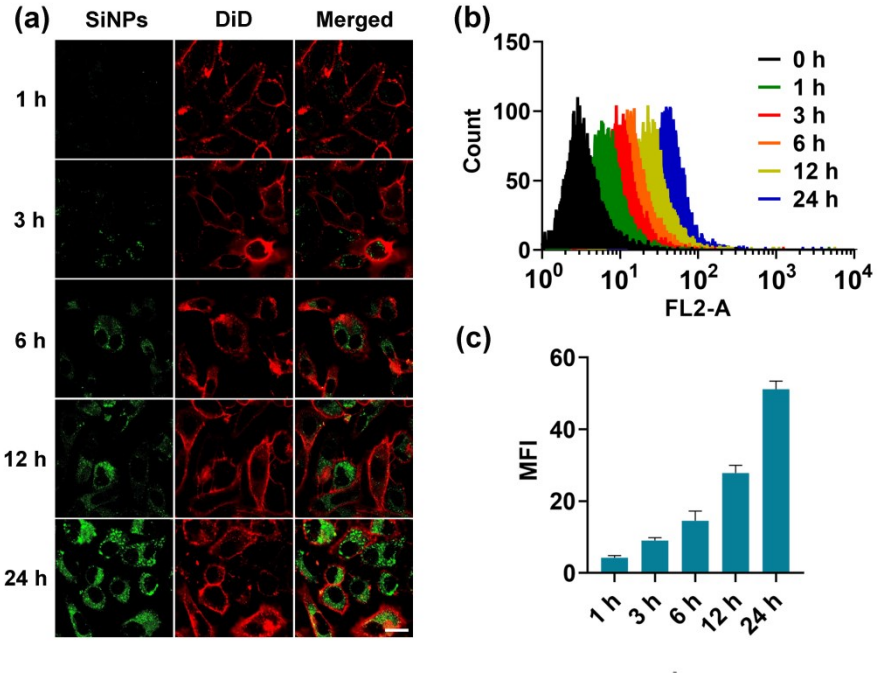

Fig. S7 Cell uptake study of SiNPs. (a) CLSM images of PC3 cells exposed to SiNPs at different time points from 1 to 24 h. The membrane was labeled with DiD (red). Scale bar = 25 μm. (b) FCM data of PC3 cells exposed to SiNPs at different time points from 0 to 24 h. (c) Semi-quantitative analysis of SiNPs absorbed by PC3 cells in (a).

We analyze the fluorescence intensity of the cells by FCM to quantify the cellular uptake of SiNPs. When the incubation time increases from 0 to 24 h, the fluorescence intensity of SiNPs in the cells is enhanced, indicating SiNPs have a time-dependent cellular uptake (Fig. S7b). CLSM is used to semi-quantitatively monitor the intracellular uptake of SiNPs. As shown in the Fig. S7a, with the incubation time increases, the fluorescence intensity in the cells is enhanced, indicating more SiNPs enter the cells. The quantitative calculation result also shows that SiNPs in the cells gradually increase with the extension of the incubation time (Fig. S7c), indicating that SiNPs have time-dependent cellular uptake.

10. Inhibition of SiNPs on HH signaling pathway in LNCaP cells

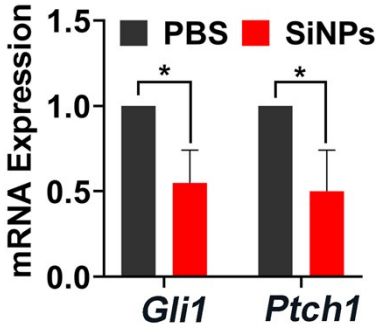

Fig. S8 Inhibition of SiNPs on HH signaling pathway in LNCaP cells. *Gli1* and *Ptch1* mRNA expression in LNCaP cells treated with 700 μg/mL SiNPs. The results are means ± SD from three independent experiments, $*P < 0.05$.

The expression of *Gli1* and *Ptch1* mRNA in LNCaP cells treated with SiNPs were significantly reduced compared to that in PBS group, indicating that SiNPs have inhibitory effect on the HH signaling pathway of LNCaP cells.

11. The high-resolution images of filopodia.

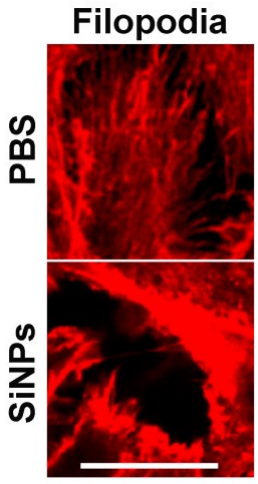

Fig. S9 The high-resolution images of filopodia. Scale bar = 25 μm

After treatment with SiNPs, filopodia showed a severe damage with an obvious shortening.

12. Wound healing of PC3 cells treated with SiNPs

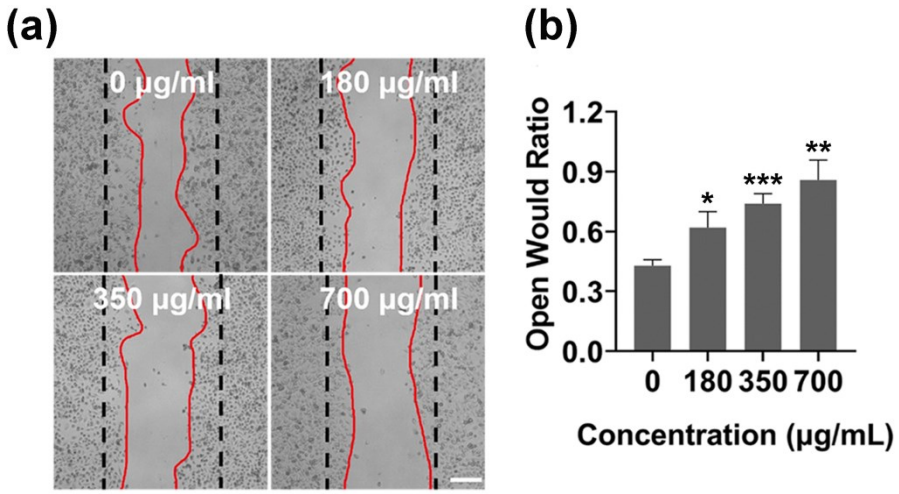

Fig. S10 Wound healing of PC3 cells treated with SiNPs. (a) Microscope images of PC3s treated with different concentrations (0, 180, 350 and 700 μg/mL) of SiNPs for 24 h after scratching. (b) Quantitative calculation result of the images in (a). Scale bar = 200 μm. The results are means ± SD from three independent experiments. *P< 0.05; **P< 0.01; ***P<0.001.

As the concentration of SiNPs increases, the open would gradually increases (Fig. S10a). The quantitative calculation result of the images shows that the inhibitory effect of SiNP on PC3 cells migration is enhanced as the concentration increases (Fig. S10b).

13. Semi-quantitative results of transwell migration and invasion

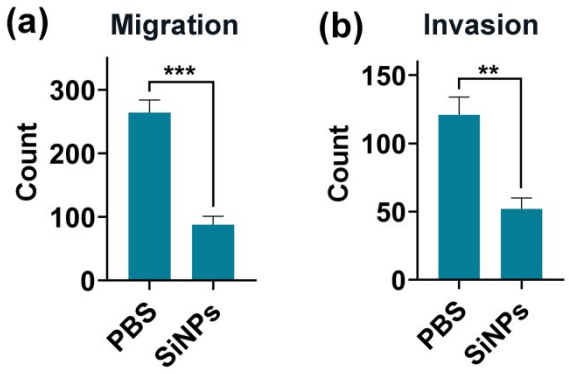

Fig. S11. Semi-quantitative results of transwell migration and invasion assays. Semi-quantitative results of transwell migration and invasion of PC3 cells treated with SiNPs.in Fig. 4e. The results are means ± SD from three independent experiments. $^{**}P < 0.01$; $^{***}P < 0.001$.

Through transwell migration (Fig. S11a) and invasion (Fig. S11b) experiments, the migration of SiNPs-treated PC3 cells is suppressed (by 33%), as well as invasion (by 43%).

14. The degree of lung metastasis in tumor model of PC3 prostate cancer.

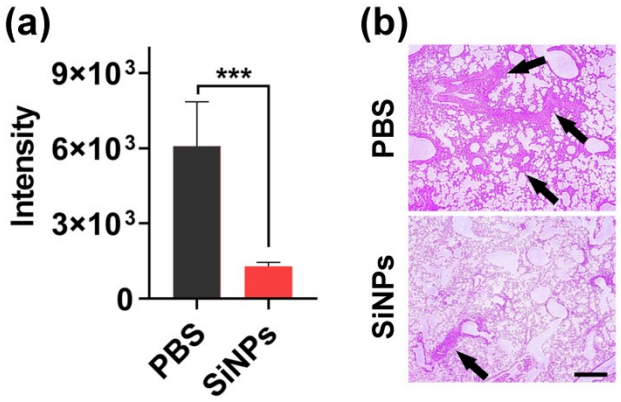

Fig. S12 The degree of lung metastasis in tumor model of PC3 prostate cancer. (a) The bioluminescence intensity of lungs in different groups in Fig. 5(c). Error bar represents the s.e.m., n = 3, ***$P < 0.001$. (b) H&E staining slices of the lungs taken from different groups. Black arrows highlight the metastatic tumors of the lungs. Scale bar = 100 μm.

The bioluminescence intensity of metastatic tumors in lungs taken from the PBS group is significantly stronger than that in the SiNPs group (Fig. S12a), indicating that the lung metastasis of the tumor is suppressed by SiNPs. H&E staining images of lungs also have consistent results (Fig. S12b).

15. *Gli1* mRNA expression at tumor site

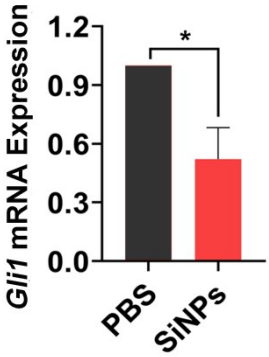

Fig. S13 *Gli1* mRNA expression at tumor site. The results are means ± SD from three independent experiments, $*P < 0.05$.

The total RNA from the tumor site is extracted to analyze, we found that the expression of the *Gli1* mRNA in the SiNPs group is significantly reduced.

16. References

1. M. S. Hayden and S. Ghosh, *Cell*, 2008, **132**, 344.
2. I. Vivanco and C. L. Sawyers, *Nat. Rev. Cancer*, 2002, **2**, 489.
3. S. Yoon and R. Seger, *Growth Factors*, 2006, **24**, 21.
4. Y. L. Zhong, F. Peng, F. Bao, S. Y. Wang, X. Y. Ji, L. Yang, Y. Y. Su, S. T. Lee and Y. He, *J. Am. Chem. Soc.*, 2013, **135**, 8350.